ARTICLES
https://doi.org/10.1038/s41588-019-0483-y

nature genetics

Corrected: Publisher Correction

Inferring whole-genome histories in large population datasets

Jerome Kelleher*, Yan Wong, Anthony W. Wohns, Chaimaa Fadil, Patrick K. Albers and Gil McVean

Inferring the full genealogical history of a set of DNA sequences is a core problem in evolutionary biology, because this history encodes information about the events and forces that have influenced a species. However, current methods are limited, and the most accurate techniques are able to process no more than a hundred samples. As datasets that consist of millions of genomes are now being collected, there is a need for scalable and efficient inference methods to fully utilize these resources. Here we introduce an algorithm that is able to not only infer whole-genome histories with comparable accuracy to the state-of-the-art but also process four orders of magnitude more sequences. The approach also provides an 'evolutionary encoding' of the data, enabling efficient calculation of relevant statistics. We apply the method to human data from the 1000 Genomes Project, Simons Genome Diversity Project and UK Biobank, showing that the inferred genealogies are rich in biological signal and efficient to process.

The mathematical concept of a tree is fundamental to evolutionary biology. From Darwin's speculative sketches[1] and Haeckel's phylogenetic imagery[2] to modern syntheses that encompass all species of life[3], trees encode and summarize the outcomes of evolutionary processes. A large number of methods now exist to infer trees[4], which are used as input for many downstream applications[5]. However, a tree can only be used to describe the ancestry of a set of DNA sequences if they are transmitted across generations as a single unit. Any process that causes different parts of a sequence to have different ancestors results in a history that cannot be described by a single tree, but instead requires a network[6]. This presents difficulties when inferring ancestry within a sexually reproducing species, in which DNA is inherited from both mother and father through recombination.

The need for structures that are more general than trees to describe ancestry has long been recognized[7]. Multiple representations of phylogenetic networks exist that model non-vertical transmission of genetic information, which arises from horizontal gene transfer and hybridization[6]. The ancestral recombination graph (ARG)[8,9] models the network that arises from inheritance within sexually reproducing species, encoding the recombination and common ancestor events in the history of a sample. In principle, ARGs contain all knowable information about genetic history and are therefore of central importance in population genetics[10–13]; however, practical applications have been limited by the prohibitive computational cost of inferring them. The problem of finding an ARG with the minimum number of recombination events required to explain a set of sample sequences cannot be solved in polynomial time[14–17] and, although non-minimal polynomial time algorithms[18,19] and various techniques to reduce search space exist[9,20,21], in practice these are too slow to apply to even moderately sized datasets. Several heuristic methods for inferring ARGs have been developed[10,22–25], although most are limited to tens of samples and a few thousand variant sites. The ARGweaver program[13] is the current state-of-the-art and a substantial advance over earlier methods, as it performs statistically rigorous inference of ARGs over tens of thousands of variant sites. However, computational time grows rapidly with the number of samples, limiting use to a few tens of samples. The widespread use of ARGs is also hindered by the lack of interchange standards and community toolkits, despite several efforts to standardize[26,27]. Consequently, the ARG remains a structure that is known to be fundamental to our understanding of the ancestry of populations, but one that is hardly ever used in practice.

Here we introduce a method—tsinfer—that removes these barriers to the adoption of ARGs in the analysis of genome variation data. Notably, tsinfer vastly expands the scale over which ancestry can be inferred, simultaneously increasing the number of variant sites and sample genomes by several orders of magnitude, with accuracy comparable to the current state-of-the-art. Moreover, we show that the data structure produced by tsinfer, the succinct tree sequence (or tree sequence, for brevity)[28,29] has the potential to store genetic data for entire populations, using a fraction of the space that would be required by current methods. As an encoding of the data based on the evolutionary history of the samples, many statistics of importance in evolutionary biology and statistical genetics can be computed efficiently using this structure. The tree sequence toolkit (or tskit) is a free and open source library providing access to these algorithms. Thus, the two main practical obstacles to using ARGs (the lack of efficient inference methods and software to process the output) have been removed. We apply tsinfer to three large-scale human datasets (the 1000 Genomes Project (TGP)[30], the Simons Genome Diversity Project (SGDP)[31] and the UK Biobank (UKB)[32]) and show how biological signals can easily be inferred from the resulting genealogical representation.

Results

Succinct tree sequences. The tangled web of ancestry that describes the genetic history of recombining organisms is conventionally encoded by common ancestor and recombination events in an ARG. The result of this process is a sequence of marginal trees, each encoding the genealogy of a particular segment of DNA[16]. Moving along a chromosome, recombination events alter the trees in a well-defined manner[17], with adjacent trees tending to be highly correlated. The succinct tree sequence is an encoding of recombinant

Big Data Institute, Li Ka Shing Centre for Health Information and Discovery, University of Oxford, Oxford, UK. *e-mail: jerome.kelleher@bdi.ox.ac.uk

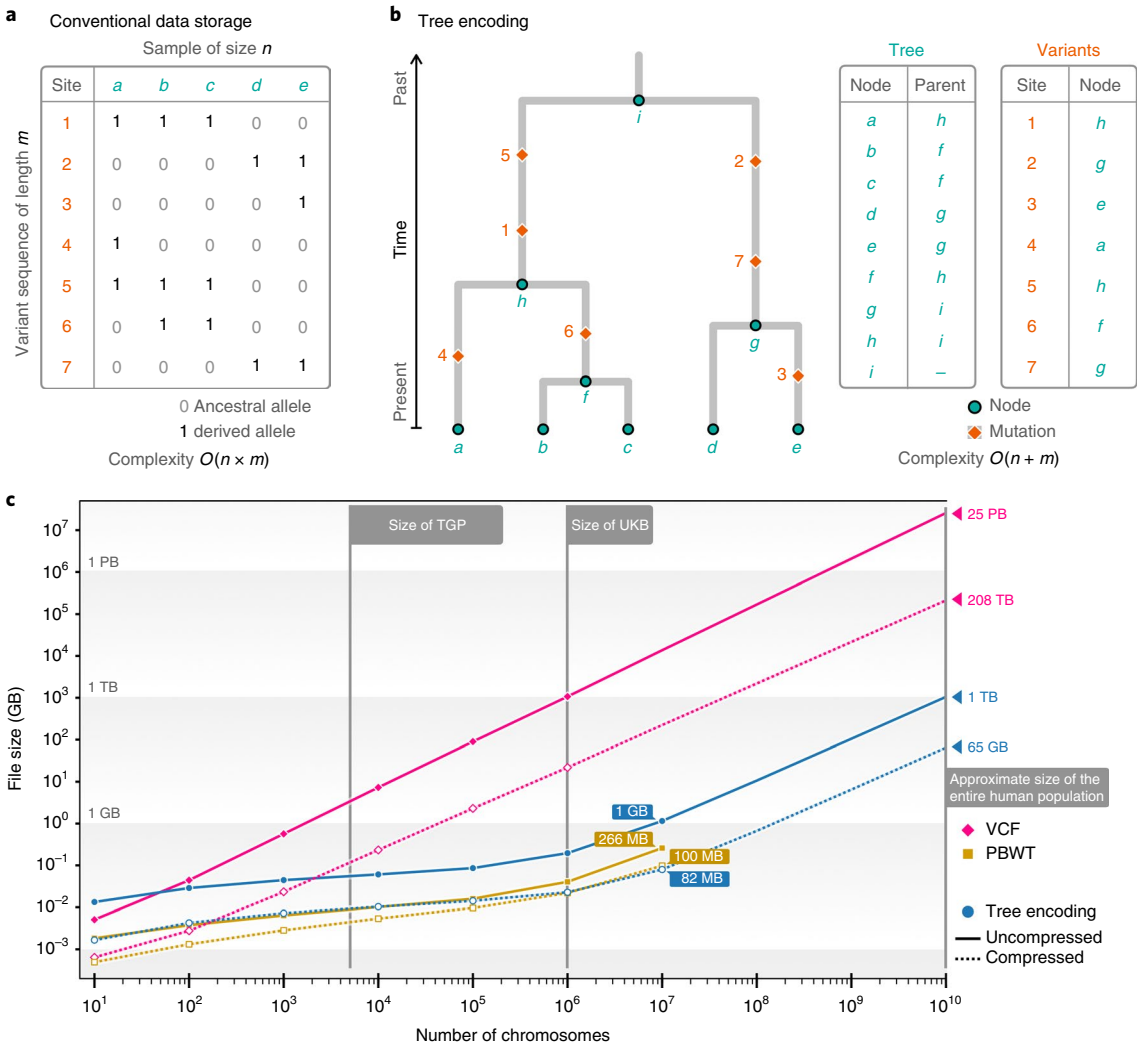

Fig. 1 | Comparison of tree sequences with standard methods for storing genetic variation data. a, The variant matrix underlying conventional storage methods for genetic variation data. **b**, A genealogical encoding of the data; if we know the tree we can store each variant site in constant space. **c**, Estimated sizes of files required to store the genetic variation data for a simulated human-like chromosome (100 Mb) for up to 10 billion haploid (5 billion diploid) samples. Simulations were run for between 10^1 and 10^7 haplotypes using msprime[28], and the sizes of the resulting files are plotted (points). In each case, we show the original tree sequence file uncompressed and compressed using tszip (retaining only the topological information that is needed to represent genotypes using the --variants-only option). We also show the corresponding variation data encoded in the VCF[35] and PBWT[36] formats, along with their gzip-compressed equivalents. The VCF files for 10^7 samples were too large and time-consuming to process. The projected file sizes for VCF and compressed VCF files are based on fitting a simple exponential model. Projected files sizes for tree sequences are based on fitting a model based on the theoretical growth of tree sequences[28]. In cases in which we extrapolated the data, the largest data point was withheld from fitting to assess the model fit. We do not extrapolate for the PBWT files, as there is no theoretical model to predict their size.

ancestry that takes advantage of this correlation structure by storing each edge shared by multiple adjacent trees exactly once[28,29]. This simple device captures shared structure among trees and leads to efficient processing algorithms[28]. The ARG, which encodes the events that occurred in the history of a sample, is formally distinct from the succinct tree sequence, which encodes the outcome of those events; although we note that it is possible to augment a tree sequence to contain all information in an ARG.

The succinct tree sequence has the potential to markedly reduce the space required to store genomic variation data. Such information is usually encoded as a matrix, with columns representing samples and rows corresponding to sites along the genome at which variation is observed (Fig. 1a). For n samples and m sites, we need $O(nm)$ space to store the matrix. Studies such as the UKB[32] contain hundreds of thousands of samples, and such large datasets are expected to become increasingly common[33]. As many species have millions of variant sites per chromosome, storing and processing such huge matrices is a major burden. Tree sequences provide an efficient alternative. The variation that we observe is the result of mutations that occurred in the ancestors of our samples. If we know the genealogy at a particular site, we can fully describe genetic variation by recording where in the ancestry these mutations arose[34] (Fig. 1b); multiple mutations at a given site are rare, and each site therefore requires $O(1)$ storage space rather than $O(n)$. Figure 1c shows the space required to store variation data for simulations of up to 10 million human-like chromosomes, extrapolated out to 10 billion. In this idealized case, storing the genotype data in the most widely used format (VCF[35]) would require 25 PB (that is, approximately 25,000 1 TB hard disks; we use binary multipliers throughout when referring to computations sizes), whereas the tree sequence encoding would require only around 1 TB. Thus, if we were able to store variation data using the tree sequence encoding, we could store and

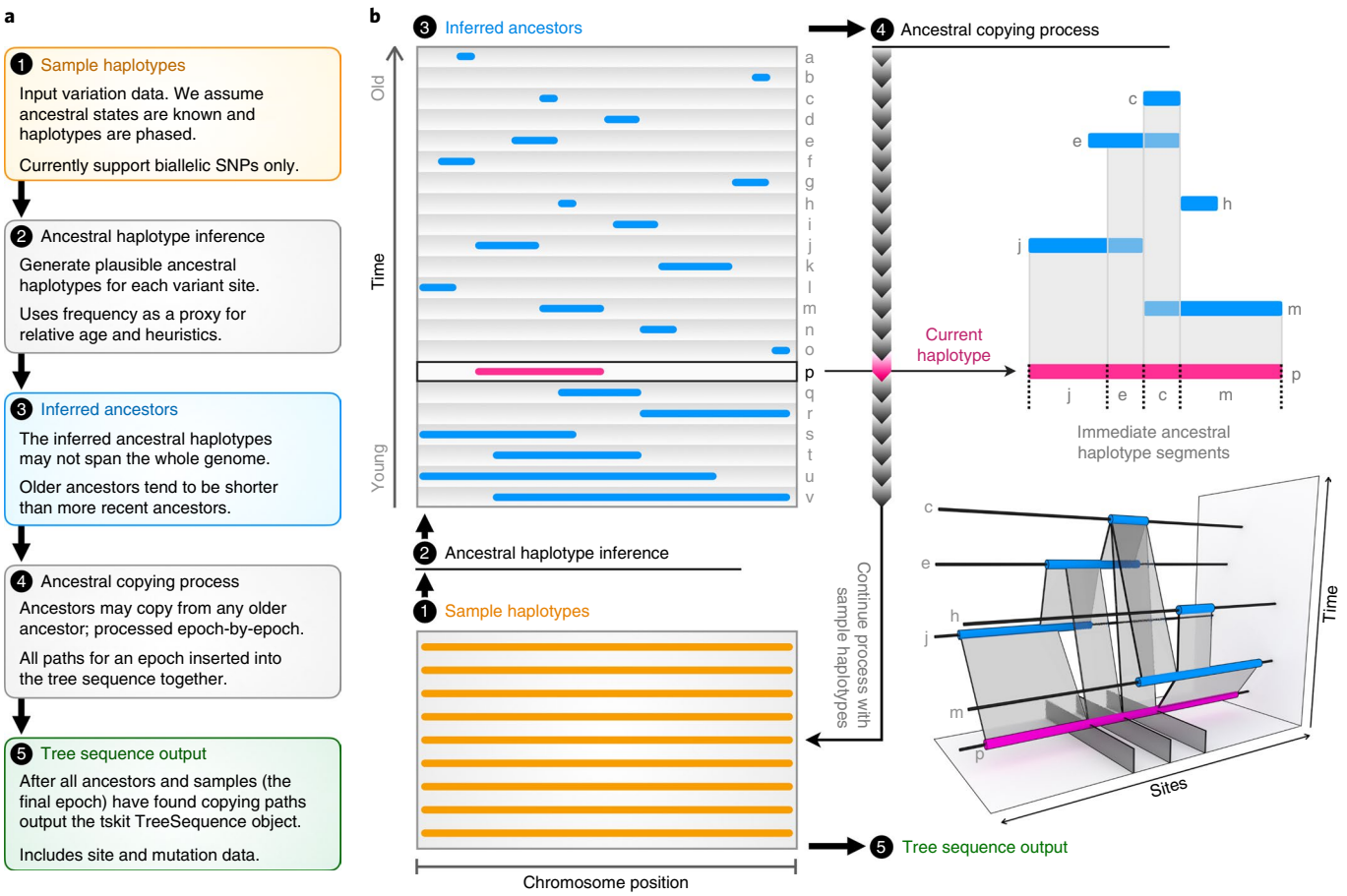

Fig. 2 | A schematic of the major steps of the inference algorithm. a, Flowchart of algorithm steps. **b**, Schematic overview. Starting from a set of sample haplotypes extending over the genome (1), we use the ancestral haplotype inference method (2) to reconstruct fragments of ancestral sequence (3), then infer copying paths among these ancestors (4). The ancestral copying process is shown on the right, using an arbitrary haplotype (*p*) for illustration. As we move from left to right along *p*, we infer that it has most recently copied from *j*, *e*, *c* and then *m*. Incorporating the copying history of all older haplotypes (for example, *m* copied partly from *c* and partly from *h*), partial coalescent trees emerge in the bottom-right panel. Once copying paths have been found for all ancestors and samples, we output a tskit tree sequence (5).

process any conceivable dataset on a present-day laptop. Existing specialized methods can also achieve much better compression levels than compressed VCF; in particular, the Positional Burrows Wheeler Transform (PBWT) is an extremely concise method of storing genotype matrices that supports efficient exact haplotype matching[36]. Notably, Fig. 1 shows that even though the compressed tree encoding also stores the full genealogy at every site (and therefore the haplotypes of every genetic ancestor), it is competitive with PBWT and even smaller at the largest scales.

Converting data into a highly compressed form usually requires costly decompression before use. A great advantage of the tree sequence encoding is that we can compute many statistics directly from the trees without decoding the genotypes. For example, computing the frequency of specific variants within subsets is a key building block of many genetic statistics. The algorithm for recovering trees from the encoded tree sequence representation allows us to compute allele frequencies far more efficiently than is possible when working with a raw matrix representation of the data[28]. Consider, for example, the largest tree sequence simulated in Fig. 1, which represents the ancestry of 10^7 chromosomes, each of which is 100 Mb long. It takes about 2.2 s to load this 1.2 GB tree sequence; around 7.5 s to iterate over all 650 thousand trees; and approximately 17 s to compute allele frequencies within an arbitrary subset of 10^6 samples at all 670 thousand sites. By contrast, just decompressing and decoding the corresponding 6.1 TB of genotype data from BCF (a more efficient binary encoding of VCF) would require an estimated 1.8 h (based on extracting the first 10 thousand variants using cyvcf2[37]). Moreover, BCF and other existing formats for storing variant data do not consider ancestry in any way. If we wished to store the actual trees from this simulation of 10^7 samples using the most efficient and popular interchange format (Newick), we would need approximately 256 TB of space and it would take an estimated 5.3 CPU years to parse (based on BioPython's[38] Newick parser—one of the most efficient available—taking about 262 s per tree).

Inference algorithm. DNA sequences can be considered mosaics of sequence fragments that have been inherited from recent ancestors through an error-prone copying process. Similarly, these ancestors are themselves mosaics, copied imperfectly from yet older ancestors. Further back in time these ancestral sequence fragments (or haplotypes) become shorter, as recombination breaks up the contributions of different ancestors over the generations. Our inference method is based on the premise that if these ancestral haplotypes were known it would be possible to infer a plausible copying history for large numbers of input DNA sequences. Notably, this approach means that we do not need to compare sample haplotypes with each other, avoiding the resulting quadratic time complexity.

We do not usually know these ancestral haplotypes, but we can attempt to infer them. If we assume that the contemporary variation that we observe at each site on the genome is the result of a

single mutation, we know that every sample haplotype that has the mutated (or derived) state at this site must have inherited it from a single ancestor. Moreover, these samples will also have inherited some fragment of the ancestral haplotype around the focal site. For mutations that arose recently, the shared haplotype will tend to be long, as recombination will not have had time to break it up. Conversely, for ancient mutations the shared ancestral haplotype will tend to be short (Fig. 2).

The first step in our algorithm is to infer ancestral haplotypes based on the variation present in the sample sequences, for which we use a simple heuristic. In brief, we first use the frequency of the derived state at each site as an approximation of the relative age of the corresponding ancestor (Supplementary Fig. 1). Then, for each ancestor we work outward from the focal site taking a consensus value among samples that carry the derived state at the focal site (see Supplementary Fig. 2 and Methods for details). Although heuristic, this method is reasonably accurate and robust to errors (Supplementary Fig. 3).

After estimating ancestral haplotypes, we then infer how they relate to each other using a variation of the Li and Stephens (LS) model[39], which regards a haplotype as an imperfect mosaic of the haplotypes in some reference panel. For a given ancestral haplotype, our reference panel consists of all older ancestral haplotypes. Because our reference haplotypes are ancestral rather than contemporary, we make a slight modification to the standard LS process: alongside the usual 0/1 states, a third haplotypic state is used to represent non-ancestral material from which copying can never occur. Computing the most likely path using the LS model allows us to estimate the immediate ancestor for each segment of DNA in the focal haplotype. Figure 2b shows an example of such a copying path for a focal haplotype and how it copies from different ancestors along its length. Once we have found copying paths for all ancestors and input sample haplotypes, we are guaranteed to have complete genealogical trees for every position along the genome, albeit ones that may contain nonbinary nodes (that is, polytomies). Furthermore, these copying paths correspond to edges in the tree sequence formulation[29], and so the copying process directly generates a succinct tree sequence. Representing the ancestral haplotypes as a tree sequence lends considerable flexibility, as it allows us to combine information from diverse sources; for example, we can use a tree sequence estimated from one dataset as ancestors for another (see 'Applications'). Encoding the inferred ancestors as an incrementally updated tree sequence also allows us to find copying paths under the LS model far more efficiently than is possible using existing approaches (see Methods).

We evaluated tsinfer for accuracy and scalability using population genetic simulations to generate ground-truth data, and compare against three other tools for ancestry inference: ARGweaver[13], Rent+[25] and fastARG (https://github.com/lh3/fastARG). Figure 3 compares the accuracy of inferred ancestral topologies; we use the Kendall–Colijn tree distance metric[40], as it is more sensitive than alternative metrics (Supplementary Fig. 4) and is robust to the presence of nonbinary nodes in trees (see Methods). We find that tsinfer is consistently more accurate than fastARG and Rent+ and has similar accuracy to ARGweaver under a range of different models of error and demography (Supplementary Figs. 5–7), while scaling to vastly larger input sizes (Supplementary Figs. 8, 9). In particular, Supplementary Fig. 7 shows that the accuracy of tsinfer is substantially higher than the accuracy of ARGweaver in the presence of a selective sweep, suggesting that our nonparametric approach is more robust to departures from the assumptions of the neutral coalescent model. See Methods for details of how these comparisons were performed.

Applications. To evaluate the performance of tsinfer on empirical data, we inferred tree sequences for three datasets on human

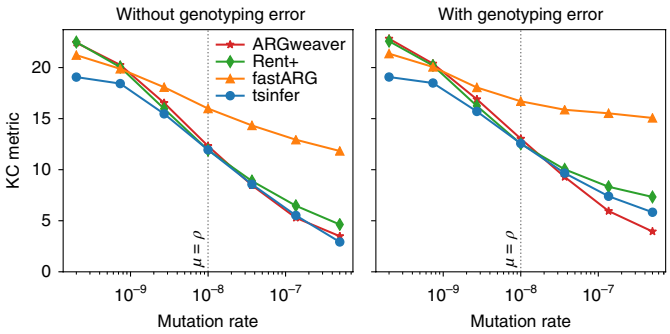

Fig. 3 | Accuracy of ancestry inference using different methods. Coalescent simulations for 16 sample haplotypes of 1 Mb in length under human-like parameters ($N_e = 5{,}000$, with recombination rate $\rho = 10^{-8}$ per base per generation) and an infinite sites model of mutation were simulated using msprime[28]. The reported tree topology distance is the Kendall–Colijn (KC) metric, weighted by the genomic distance spanned by each tree. Each point is the average of 100 independent replicates at a given mutation rate. The point at which the mutation rate is equal to recombination rate (similar to humans) is marked with a vertical dotted line. Standard errors are smaller than the plotted symbols in all cases. Note, lower values indicate greater accuracy.

chromosome 20: the TGP, which consists of low-coverage whole-genome sequencing data from 2,504 individuals across 26 worldwide populations[30]; the SGDP, which consists of high-coverage sequencing data from 278 individuals from 142 worldwide populations[31]; and the UKB, consisting of SNP array data from 487,327 individuals from the United Kingdom[32]. Table 1 summarizes input data, inferred tree sequences and computing resources required. For UKB, we considered multiple strategies, augmenting the data with ancestors inferred from TGP and subsets of haplotypes from the UKB itself as potential ancestors. For each dataset, we used statistically inferred haplotypes as input.

Across chromosome 20, the TGP data consisted of 860 thousand sites after filtering (see Methods for details). After inferring ancestors and matching sample haplotypes to these ancestors, we obtained a 297 MB tree sequence (46 MB compressed, compared to the 141 MB BCF encoding of the same genotypes). Under the standard neutral model, we expect the number of distinct trees to be roughly equal to the number of variable sites within human data, and the number of edges to be roughly four times the number of trees[28,29]. We observe similar numbers of distinct trees (550 thousand) as filtered sites (860 thousand, from 1.8 million unfiltered), but the number of edges is 7.3 million, which is greater than expected and suggests that the differences between adjacent inferred trees are larger than expected under idealized conditions. Loading the tree sequence required approximately 3 s; iterating over all 550 thousand trees around 0.6 s; and decoding all genotypes approximately 9 s. In comparison, decoding the same genotypes from BCF required around 15 s using cyvcf2. The SGDP data consisted of 348 thousand sites after filtering, and this resulted in an 83 MB tree sequence (11 MB compressed, compared to the 11 MB BCF encoding of the same genotypes). Loading the tree sequence required approximately 1.6 s; iterating over all 196 thousand trees around 0.1 s; and decoding all genotypes approximately 1.8 s. These results demonstrate the feasibility of representing existing datasets through tree sequences, with file sizes that are comparable to current standards and excellent analytical accessibility.

To assess the validity of the inferred tree sequences, we computed a series of metrics summarizing reconstructed ancestral relationships. We first calculated the number of edges for each sample, which measures the extent to which the genome of an individual can be compressed against the inferred ancestors. In TGP, samples

Table 1 | Summary of input data, output tree sequences and computing resources required for TGP, SGDP and UKB chromosome 20

	Input			Output				Resources	
	n	Sites	Size	Nodes	Edges	Trees	Size	Time	RAM
SGDP	277	348×10^3	15 MB	236×10^3	1.7×10^6	196×10^3	83 MB	5 min	3.6 GB
TGP	2,504	860×10^3	135 MB	735×10^3	7.3×10^6	550×10^3	296 MB	2 h	11 GB
UKB	487×10^3	15.8×10^3	1.6 GB	1.9×10^6	484×10^6	15.8×10^3	14.5 GB	3 h	160 GB
UKB + TGP	487×10^3	15.6×10^3	1.6 GB	5.5×10^6	185×10^6	15.6×10^3	5.8 GB	15 h	66 GB
UKB + UKB	487×10^3	15.8×10^3	1.6 GB	2.0×10^6	62×10^6	15.8×10^3	2.1 GB	50 h	40 GB

Input sizes reported are for the input .samples files of tsinfer, which uses the Zarr library (https://zarr.readthedocs.io/) to achieve similar compression levels to BCF. The times reported are the total time required to produce the output tree sequence from the .samples file on a server with two Xeon Gold 6148 CPUs (40 cores in total; no hyperthreading) and 187 GB of RAM. For the separate analyses of SGDP, TGP and UKB, we used the standard tsinfer inference pipeline. For the combined analyses of UKB and TGP, we matched the UKB samples to the inferred TGP tree sequence (time reported is just for sample matching phase). For the analysis of UKB and UKB, we incrementally added samples from UKB to the ancestors inferred from UKB (see text).

have an average of 648 edges (with a median length of 44 kb and an average N50 of 236 kb), with those of African ancestry having a greater number (750) than those of European (551) or Asian (665) ancestry (Supplementary Figs. 10a, 11). These findings are likely to primarily reflect known differences in the long-term effective population size, although the findings will also be affected by sampling strategy and error modes. We find higher values in SGDP that reflect the lower sample sizes (overall average: 1,113 edges, African ancestry: 2,178, European ancestry: 803 and Asian ancestry: 879; Supplementary Figs. 10b, 12). In both datasets we identified a few outlier samples with very high edge counts, suggesting error (see Supplementary Note).

We next considered whether the inferred tree sequences could be used to characterize ancestral relationships in TGP and SGDP by computing, for each individual, the population distribution of their genealogical nearest neighbors (GNN). Given K sets of reference nodes (for example, the samples for each of the 26 TGP populations), the GNN statistic for a specific node is a K vector that describes the proportion of its immediate neighbors within the tree from each of these reference sets (see Methods). We find that, despite the noise generated by uncertainty in tree reconstruction (manifested as polytomies), the chance nature of the genealogical process and data error, the tree sequences can characterize global population structure (Fig. 4a, b), within-population relatedness (Fig. 4c), and identify regions of differential ancestry within an individual (Fig. 4d). These analyses demonstrate the potential of interrogating the inferred genealogical structure at different resolutions to describe both broad and fine-scale patterns in contemporary human genomic diversity.

Finally, to assess the performance of tsinfer on vast datasets, we analyzed the approximately 500 thousand individuals for which data are available in the UKB. The sparsity of variant sites and inherent lack of rare variants in the UKB SNP array data is insufficient to accurately infer ancestors using the standard algorithm. Therefore, we considered two alternative strategies: using ancestors estimated from other data and using subsets of the sample to act as proxies for ancestors. In the first approach, we matched the UKB haplotypes to the tree sequence inferred for TGP, generating a 5.8 GB tree sequence (740 MB compressed). Supplementary Figure 13 shows the self-reported ancestry in UKB tallies with TGP GNN values and adds granularity. Furthermore, by analyzing the copying patterns in this tree sequence, we found nine individuals who are likely to be in both the TGP and UKB datasets (see Supplementary Note).

Our second strategy for improving ancestor inference involves sequentially adding subsets of the sample itself as potential ancestors. By iteratively adding samples, the approach of generating putative ancestors from shared recombination breakpoints (path compression; see Methods) constructs many more ancestors than would be possible if all samples were added simultaneously. Thus, we began by updating the tree sequence of the ancestor with the paths of two arbitrarily chosen samples; then updating the resulting tree sequence with the paths taken for four other samples; and then again for eight; and so on up to 131,072. After matching all 1 million sample haplotypes against these augmented ancestors, we obtained a 2.1 GB tree sequence (318 MB compressed, compared to the equivalent 1.4 GB BCF file). Loading this tree sequence required approximately 9 s and iterating over all 15.8 thousand trees takes around 11 s. Decoding genotypes for the first 1,000 sites required 9.5 s; in comparison, decoding the genotypes for the first 1,000 sites in the original BGEN file using the bgen C library required 49 s. Analysis of the GNN structure of the tree sequence (Fig. 5) demonstrates strong geographical clustering of relatedness at this level of resolution, with connections between birth locations reflecting geographical proximity. Although signals of population structure are evident here, further work is required to understand the implications for the statistical analysis of association and other applications.

Discussion

Inferring genealogical relationships from patterns of genomic variation is a long-standing problem in evolutionary biology that connects to the fundamental forces and events that shape a species. However, our ability to infer such histories has been limited by the computational complexity of the problem. The work presented here represents a major advance by providing a principled, yet scalable approach that can be applied to datasets of unprecedented size. Although the algorithms presented are both heuristic and deterministic, the approach of breaking down the problem into inferring relative variant age, ancestral haplotypes and the genealogical relationships between these ancestors results in a modular framework that scales to vast sample sizes (Supplementary Fig. 9). Moreover, each component can be improved independently, potentially accommodating uncertainty through stochastic approaches.

Nevertheless, the method does make a number of fundamental assumptions. First, we assume that each variant in a population has a single mutational origin. Although this is unlikely to be true in practice (particularly in large samples), our ancestor estimation method is likely to find the dominant ancestral haplotype. Recurrent and back mutations will therefore not be handled well by the current algorithm, although this could in principle be addressed by iterative approaches. Second, we assume that frequency is a proxy for relative variant age. Importantly, our algorithms only require accuracy about relative age within genealogically connected parts of the tree sequence. Under simple demographic models, we estimate that relative frequency indicates relative age for roughly 90% of closely located pairs of variants (Supplementary Fig. 1). In theory, methods for dating genomic variants could be used to improve ancestor estimation and also assign dates to nodes within the tree sequence, although these remain unresolved problems. Third, we

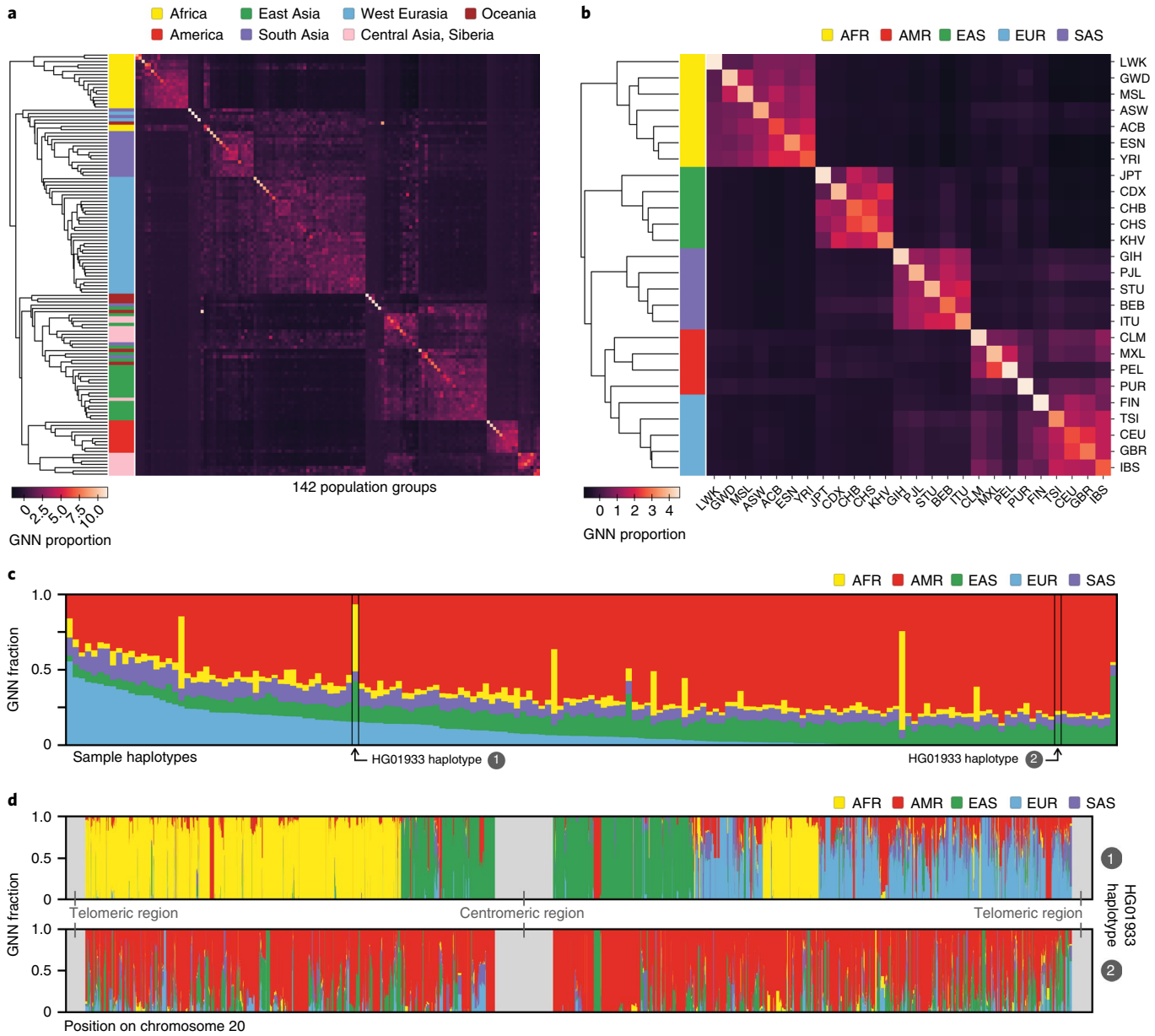

Fig. 4 | Tree sequence characterization of global genome diversity. a, *Z*-score-normalized GNN proportions for SGDP by population ($n = 278$ individuals). The GNN matrix was first *z*-score normalized by column and the rows were then hierarchically clustered. See Supplementary Fig. 16 for a larger version with population labels. **b**, As for **a**, but for the TGP data ($n = 2{,}504$ individuals). AFR, Africa; AMR, America; EAS, east Asia; EUR, Europe; SAS, south Asia; population codes are TGP abbreviations[30]. **c**, Average GNN proportions for all individuals within the Peruvian population in TGP. Colors indicate continental-level groupings. **d**, The GNN proportions across the chromosome for the two haplotypes of HG01933, from the Peruvian population in TGP. HG01933 was chosen as an example of an individual who showed evidence of very recent admixture from multiple source populations. We note that apparent short tracts of different ancestry most likely do not reflect true changes in recent ancestry, but arise through the stochastic nature of genealogical processes and errors in inference.

assume that the ratio of mutation to recombination is sufficiently high to use mutations as the starting point for ancestor inference. However, the path compression approach used here (see Methods) identifies additional ancestors through shared recombination events and, within the SNP array analysis of the UKB data, performs well, compensating for the low variant density and lack of rare variants. Finally, the current methodology works well for low error rates, but its performance is reduced (typically characterized by an excess of edges) by genotyping and, in particular, haplotype phasing errors. In the future, population-scale high-coverage and routine long-read genome sequencing will reduce the source of such errors and it may be feasible to construct steps of the algorithm that are more robust than those currently implemented. Our method does not estimate the times of internal tree nodes beyond a simple ordering, which is an important limitation in terms of evolutionary analyses. Inferring node times conditioned on a tree sequence topology—at scale—is therefore an important goal for future work.

Tree sequences have many potential applications. The most obvious is as an efficient lossless storage format for population-scale datasets. Although compression performance on simulated data (Supplementary Figs. 14, 15) is close to the theoretical possibilities shown in Fig. 1, the compression of real data by tsinfer does not currently fulfill this potential. More careful modeling of the complexities of genetic data—in particular the various error modes—will

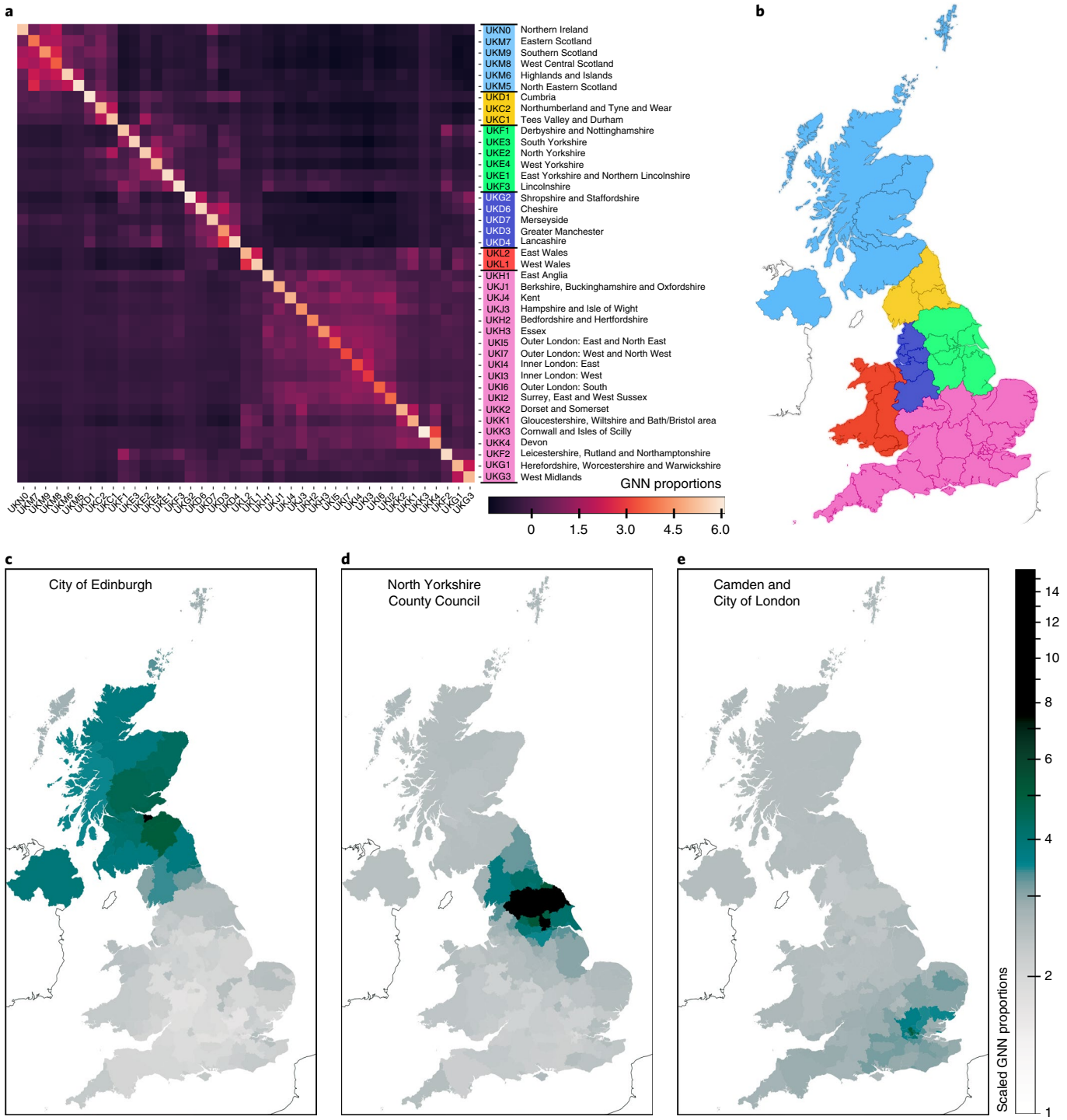

Fig. 5 | Tree sequence characterization of the UKB data. a). Normalized GNN proportions for 628,651 haplotypes self-reported as born in Britain or Northern Ireland (the 262,136 sample haplotypes used for ancestor augmentation were removed from this analysis) calculated relative to birth location (grouped according to NUTS 2018, level 2; see Methods), that is, reporting the fraction of the GNNs of each sample who were born in a given geographical area. The columns in the GNN matrix were *z*-score normalized before the rows were hierarchically clustered. **b**, Geographical areas color-coded by group clustering. The six areas correspond to the first six clusters obtained by hierarchical clustering of the 41 birth locations in **a**. **c**–**e**, GNN proportions computed for specific NUTS level 3 areas. **c**, City of Edinburgh ($n = 7{,}571$ individuals). **d**, North Yorkshire County Council ($n = 3{,}416$ individuals). **e**, Camden and City of London ($n = 4{,}726$ individuals). For each area, the GNN proportions were computed over 170 geographical areas (169 NUTS-3 areas and Northern Ireland). The *z*-scored proportions were translated and log-normalized. The tree sequence constructed by iteratively augmenting ancestors (see text) was used as the basis for plots (**a**–**e**).

likely be required to effectively compress millions of whole genomes. Nonetheless, compression performance is comparable to existing formats while providing exceptional analytical accessibility. Recent, unpublished work on data compression using a genealogically informed PBWT[41] also offers a related and promising approach to genome-scale inference of tree sequence topologies. The integration

of genealogical relationships with genomic variation data has value beyond population and personal genetics, for example in potentially correcting for the differential geographical confounding of rare and common variants in genetic association, and, as Speidel et al.[42] have shown, enables powerful inference of underlying evolutionary events, processes and parameters, such as mutation age, natural selection and ancient contacts between populations. Moreover, our combined analysis of the UKB and TGP datasets demonstrates the potential of also using tree sequences to integrate data sources and, more generally, to build a reference tree sequence structure for human genomic variation that can be updated as new variants are discovered. Such a structure, coupled with efficient algorithms that make use of the tree sequence could enable (and make optimally powerful) diverse statistical genetic operations including genotype refinement, genotype imputation and haplotype phasing. It could also be used to share data effectively and in a manner that preserves privacy, by describing datasets in terms of inferred ancestors rather than individual samples.

Online content

Any methods, additional references, Nature Research reporting summaries, source data, statements of code and data availability and associated accession codes are available at https://doi.org/10.1038/s41588-019-0483-y.

Received: 20 February 2019; Accepted: 15 July 2019;
Published onl Published online: 02 September 2019

References

1. Darwin, C. *Charles Darwin's Notebooks, 1836–1844: Geology, Transmutation of Species, Metaphysical Enquiries* (Cambridge Univ. Press, 1987).
2. Haeckel, E. *Generelle Morphologie der Organismen* (G. Reimer, 1866).
3. Hinchliff, C. E. et al. Synthesis of phylogeny and taxonomy into a comprehensive tree of life. *Proc. Natl Acad. Sci. USA* **112**, 12764–12769 (2015).
4. Felsenstein, J. *Inferring Phylogenies* (Sinauer Associates, 2004).
5. Yang, Z. & Rannala, B. Molecular phylogenetics: principles and practice. *Nat. Rev. Genet.* **13**, 303–314 (2012).
6. Morrison, D. A. Genealogies: pedigrees and phylogenies are reticulating networks not just divergent trees. *Evol. Biol.* **43**, 456–473 (2016).
7. Ragan, M. A. Trees and networks before and after Darwin. *Biol. Direct* **4**, 43 (2009).
8. Griffiths, R. C. The two-locus ancestral graph. *Lect. Notes Monogr. Ser.* **18**, 100–117 (1991).
9. Griffiths, R. C. & Marjoram, P. Ancestral inference from samples of DNA sequences with recombination. *J. Comput. Biol.* **3**, 479–502 (1996).
10. Minichiello, M. J. & Durbin, R. Mapping trait loci by use of inferred ancestral recombination graphs. *Am. J. Hum. Genet.* **79**, 910–922 (2006).
11. Arenas, M. The importance and application of the ancestral recombination graph. *Front. Genet.* **4**, 206 (2013).
12. Gusfield, D. *ReCombinatorics: the Algorithmics of Ancestral Recombination Graphs and Explicit Phylogenetic Networks* (MIT Press, 2014).
13. Rasmussen, M. D., Hubisz, M. J., Gronau, I. & Siepel, A. Genome-wide inference of ancestral recombination graphs. *PLoS Genet.* **10**, e1004342 (2014).
14. Bordewich, M. & Semple, C. On the computational complexity of the rooted subtree prune and regraft distance. *Ann. Comb.* **8**, 409–423 (2005).
15. Wang, L., Zhang, K. & Zhang, L. Perfect phylogenetic networks with recombination. *J. Comput. Biol.* **8**, 69–78 (2001).
16. Hein, J. Reconstructing evolution of sequences subject to recombination using parsimony. *Math. Biosci.* **98**, 185–200 (1990).
17. Song, Y. S. & Hein, J. Constructing minimal ancestral recombination graphs. *J. Comput. Biol.* **12**, 147–169 (2005).
18. Gusfield, D., Eddhu, S. & Langley, C. Optimal, efficient reconstruction of phylogenetic networks with constrained recombination. *J. Bioinform. Comput. Biol.* **02**, 173–213 (2004).
19. Gusfield, D., Bansal, V., Bafna, V. & Song, Y. S. A decomposition theory for phylogenetic networks and incompatible characters. *J. Comput. Biol.* **14**, 1247–1272 (2007).
20. Kuhner, M. K., Yamato, J. & Felsenstein, J. Maximum likelihood estimation of recombination rates from population data. *Genetics* **156**, 1393–1401 (2000).
21. Fearnhead, P. & Donnelly, P. Estimating recombination rates from population genetic data. *Genetics* **159**, 1299–1318 (2001).
22. Song, Y. S., Wu, Y. & Gusfield, D. Efficient computation of close lower and upper bounds on the minimum number of recombinations in biological sequence evolution. *Bioinformatics* **21**, i413–i422 (2005).
23. Parida, L., Melé, M., Calafell, F., Bertranpetit, J. & The Genographic Consortium Estimating the ancestral recombinations graph (ARG) as compatible networks of SNP patterns. *J. Comput. Biol.* **15**, 1133–1153 (2008).
24. O'Fallon, B. D. ACG: rapid inference of population history from recombining nucleotide sequences. *BMC Bioinformatics* **14**, 40 (2013).
25. Mirzaei, S. & Wu, Y. RENT+: an improved method for inferring local genealogical trees from haplotypes with recombination. *Bioinformatics* **33**, 1021–1030 (2016).
26. Cardona, G., Rosselló, F. & Valiente, G. Extended Newick: it is time for a standard representation of phylogenetic networks. *BMC Bioinformatics* **9**, 532 (2008).
27. McGill, J. R., Walkup, E. A. & Kuhner, M. K. GraphML specializations to codify ancestral recombinant graphs. *Front. Genet.* **4**, 146 (2013).
28. Kelleher, J., Etheridge, A. M. & McVean, G. Efficient coalescent simulation and genealogical analysis for large sample sizes. *PLoS Comput. Biol.* **12**, e1004842 (2016).
29. Kelleher, J., Thornton, K. R., Ashander, J. & Ralph, P. L. Efficient pedigree recording for fast population genetics simulation. *PLoS Comput. Biol.* **14**, e1006581 (2018).
30. The 1000 Genomes Project Consortium A global reference for human genetic variation. *Nature* **526**, 68–74 (2015).
31. Mallick, S. et al. The Simons Genome Diversity Project: 300 genomes from 142 diverse populations. *Nature* **538**, 201–206 (2016).
32. Bycroft, C. et al. The UK Biobank resource with deep phenotyping and genomic data. *Nature* **562**, 203–209 (2018).
33. Stephens, Z. D. et al. Big data: astronomical or genomical? *PLoS Biol.* **13**, e1002195 (2015).
34. Ané, C. & Sanderson, M. J. Missing the forest for the trees: phylogenetic compression and its implications for inferring complex evolutionary histories. *Syst. Biol.* **54**, 146–157 (2005).
35. Danecek, P. et al. The variant call format and vcftools. *Bioinformatics* **27**, 2156–2158 (2011).
36. Durbin, R. Efficient haplotype matching and storage using the positional Burrows–Wheeler transform (PBWT). *Bioinformatics* **30**, 1266–1272 (2014).
37. Pedersen, B. S. & Quinlan, A. R. cyvcf2: fast, flexible variant analysis with Python. *Bioinformatics* **33**, 1867–1869 (2017).
38. Cock, P. J. A. et al. Biopython: freely available Python tools for computational molecular biology and bioinformatics. *Bioinformatics* **25**, 1422–1423 (2009).
39. Li, N. & Stephens, M. Modeling linkage disequilibrium and identifying recombination hotspots using single-nucleotide polymorphism data. *Genetics* **165**, 2213–2233 (2003).
40. Kendall, M. & Colijn, C. Mapping phylogenetic trees to reveal distinct patterns of evolution. *Mol. Biol. Evol.* **33**, 2735–2743 (2016).
41. Shchur, V., Ziganurova, L. & Durbin, R. Fast and scalable genome-wide inference of local tree topologies from large number of haplotypes based on tree consistent PBWT data structure. Preprint at *bioRxiv* https://doi.org/10.1101/542035 (2019).
42. Speidel, L., Forest, M., Shi, S. & Myers, S. R. A method for genome-wide genealogy estimation for thousands of samples. *Nat. Genet.* https://doi.org/10.1038/s41588-019-0484-x (2019).

Acknowledgements

This research was conducted by using the UK Biobank Resource under application number 12788. This work was supported by the Wellcome Trust grant 100956/Z/13/Z to G.M. A.W.W. and C.F. thank the Rhodes Trust for their support. We thank J. Novembre and P. Ralph for comments on earlier drafts of this manuscript; P. Ralph and K. Thornton for many useful discussions on tree sequence algorithms. Computation used the Oxford Biomedical Research Computing (BMRC) facility, a joint development between the Wellcome Centre for Human Genetics and the Big Data Institute supported by Health Data Research UK and the NIHR Oxford Biomedical Research Centre. The views expressed are those of the authors and not necessarily those of the NHS, the NIHR or the Department of Health.

Author contributions

We used the CRediT taxonomy for contributions (https://casrai.org/credit). J.K.: Conceptualization, Data curation, Formal analysis, Investigation, Methodology, Resources, Software, Supervision, Validation, Visualization, Writing—original draft, Writing—review & editing. Y.W.: Conceptualization, Data curation, Formal analysis, Investigation, Methodology, Resources, Software, Supervision, Validation, Visualization, Writing—original draft, Writing—review & editing. A.W.W.: Formal analysis, Investigation, Validation, Visualization,

Writing—review & editing. C.F.: Data Curation, Formal analysis, Visualization, Writing—review & editing. P.K.A.: Data curation, Resources, Visualization, Writing—review & editing. G.M.: Conceptualization, Funding acquisition, Methodology, Supervision, Writing—original draft, Writing—review & editing.

Competing interests

G.M. is a shareholder in and non-executive director of Genomics PLC, and is a partner in Peptide Groove LLP. The remaining authors declare no competing interests.

Additional information

Supplementary information is available for this paper at https://doi.org/10.1038/s41588-019-0483-y.

Reprints and permissions information is available at www.nature.com/reprints.

Correspondence and requests for materials should be addressed to J.K.

Publisher's note: Springer Nature remains neutral with regard to jurisdictional claims in published maps and institutional affiliations.

© The Author(s), under exclusive licence to Springer Nature America, Inc. 2019

Methods

Age of alleles. The first step in our algorithm is to estimate the relative time at which the mutation for each variant arose (we are assuming a single origin for each mutation). Classical results in population genetics provide a theoretical expectation for the age of an allele based on its frequency[43,44]. There are several existing methods for estimating the age of alleles, but these methods are either computationally expensive or require detailed knowledge about historical population processes[45–47], although a more efficient non-parametric method has recently been introduced[48].

If we are interested in estimating topologies, however, we do not need precise estimates of the age of an allele: all we require is the order in which nodes occur. The frequency of alleles provides a computationally inexpensive way of ordering the ages of the alleles, which is surprisingly accurate for our purposes (Supplementary Fig. 1), as we only need the relative age ordering of alleles to be locally accurate. If variants on opposite ends of a chromosome are incorrectly ordered it makes little difference to the outcome of our algorithms, as the ancestral haplotypes that are involved are unlikely to overlap. By default tsinfer uses frequency as a proxy for relative allele age; however, we also allow external sources for the age of the alleles to be provided as input.

Inferring ancestral haplotypes. Once we have assigned an age order to sites, the next step in our inference process is to generate a set of putative ancestral haplotypes. We assume that there are two alleles at every site: the ancestral state, which was inherited from the ancestor of the entire population, and the derived state, which is the result of a mutation that occurred in the ancestor of the samples that carry this allele. We assume that these ancestral and derived states have been identified using existing methods[49]. Each variant site is therefore the result of a mutation that occurred in an ancestor: samples that inherit from this ancestor have the derived state, and the rest carry the ancestral state. By definition this ancestor carries the derived state at the site in question; our task then is to reconstruct the state of the ancestor around this focal site.

For a given focal site ℓ let S be the set of samples that carry the derived state. We are attempting to reconstruct the ancestral haplotype a on which the mutation occurred, and so we begin by setting $a_\ell = 1$, following the usual convention of labeling the ancestral state for a site 0 and the derived state 1. For all other sites $1 \leq k \leq m$, $k \neq \ell$ we set $a_k = -1$, indicating non-ancestral material that cannot be copied from; these non-ancestral values will be overwritten for sites around ℓ for which we can estimate the state of the ancestor. We then work to the left and right along the sequence from ℓ independently, computing the state of the ancestor at each site. The set S initially contains the samples that we believe descend from the current ancestor (assuming infinite sites and no error), and we use this set to compute a plausible state at other sites. As recombination modifies the tree topology, we update S to remove samples that are no longer in the clade induced by the focal site. We stop moving left or right from the focal site when we judge that we no longer have sufficient information to construct the ancestral haplotype. We use heuristics to determine when to remove a particular sample from S and when to end the ancestral haplotype.

Supplementary Figure 2 illustrates a simplified example of this process, showing the ancestral haplotype estimated at the focal site 8. We begin by setting $S = \{e, f, g, h\}$, that is, the set of samples that carry the derived allele at site 8. We then proceed to the right, considering each site in turn. For younger sites, the corresponding mutation cannot have occurred yet by definition, and so we always set the ancestor to 0 at these sites (for example, sites 9 and 10). When we reach a site that is older than the focal one, we compute a plausible value for our ancestor by taking the consensus among the samples in S. For example, at site 11 the estimated value for the ancestor is 1 because all haplotypes in S carry 1; similarly, at site 13, three of four samples in S carry 1, and so the consensus is 1 (the consensus can also be 0, as in site 4). We interpret disagreement with the consensus value as evidence that the samples in question have recombined away to another part of the tree. Thus, after we compute the state of the ancestor at a site, we remove any samples from S that conflict with this consensus (but see below for a slight modification used in practice). In the example, we therefore remove h at site 13 and g at site 17. We continue to the right in this way until we determine that we have insufficient information to accurately estimate ancestors. The heuristic that we have chosen is to stop when the size of S is less than or equal to half of its original size. After completing the rightward scan, we repeat the process independently leftward.

Variants with an age equal to the focal mutation are considered to be younger than the focal site (and hence always assigned the ancestral state) except in one special case. If several sites exist with a precisely equal distribution of genotypes, we assume that these all arose on a single branch of the tree and that no recombination occurred between these sites. We therefore compute consensus values for older sites between these identical focal sites in the usual way, but we do not update S when conflicts occur (assuming these to be caused by error). Once outside of the region enclosed by the identical sites, the process outlined above resumes and we update S in the usual way.

Although this method is approximate and heuristic, it generates surprisingly accurate ancestors. Supplementary Figure 3 shows a plot of the lengths of the estimated compared with the true ancestors from simulations, color-coded by the accuracy of the estimated states. We find that there is a strong bias towards ancestral haplotypes being longer than the truth; this is by design, as long haplotypes can be compensated for by the copying process, but short haplotypes cannot. Inferred haplotypes are also quite accurate, with many ancestors being inferred perfectly. Genotyping errors can result in many generated ancestors being too short, as errors often lead to samples being prematurely removed from S. To add some resilience to this, we include a slight 'dampening' to our removal rule: we remove a sample from S only if it disagrees with the consensus at two consecutive older sites. Supplementary Figure 3 shows that this slightly more complex heuristic used in practice is reasonably robust to genotyping errors.

Copying process. The LS model[39] is important for many techniques in population genomics[50]. Given an input haplotype with m sites and a reference panel of n haplotypes, the most likely copying path under the LS model is found using the Viterbi algorithm, which proceeds iteratively over sites. At each site, we compute the maximum likelihood that the input haplotype has copied from a particular reference haplotype given their states and the maximum likelihood values at the previous site; the particular form of the LS model allows this to be done in $O(n)$ time. Once the last site is reached, the most likely reference haplotype at the end of the sequence is identified, then the algorithm traces back through sites, switching to other haplotypes where required. The overall time complexity is therefore $O(nm)$ to find a copying path for an input haplotype, as we must compare with all n reference haplotypes at each of the m sites. In tsinfer the reference panel is the set of inferred ancestral haplotypes. Because there may be a different ancestor for every site, $n \approx m$, hence the time complexity of finding a copying path is $O(m^2)$. Modern sequencing datasets contain millions of variant sites, thus standard LS methods are not feasible. Moreover, in tsinfer, haplotypes can only copy from older haplotypes and the reference panel must be updated dynamically; algorithms that require a linear-time preprocessing step[50] are therefore also not feasible.

To solve this problem, we use the LS model on the tree sequence directly. Each copying path generated is equivalent to a set of edges in a tree sequence[29], in which the child is the focal haplotype and the parents are ancestors. Forwards in time (that is towards the present), we are therefore incrementally building a tree sequence. We use this partially built tree sequence as the substrate for computing LS copying paths for subsequent ancestors. The computational properties of the tree sequence data structure allow us to find exact copying paths far more efficiently than using standard methods.

The algorithm for computing Viterbi paths using a tree sequence works in the same way as the standard method. We proceed iteratively over sites, computing the maximum likelihood when copying from each ancestor at each site and recording the locations of potential recombination events. Once the last site is reached, trace-back proceeds as before, resolving a full copying path. The difference when using tree sequences is that we avoid needing to compute and store a likelihood for each reference haplotype by using the tree sequence to compress the associated likelihoods. Each ancestor corresponds to a node in the marginal tree at a given site, thus we compress the likelihoods by marking any node that has the same likelihood as its parent with a special value. Because the likelihood values are driven by the underlying tree structure of the data, they tend to cluster on the partially inferred trees and therefore compress well. Updating the likelihoods at a given site is then straightforward. We compute the likelihood for each node by reasoning about the state of the input haplotype and the location of the site's mutation in the tree. Having updated the likelihoods for the nodes corresponding to the compressed subtrees, we then recompress to take into account the new likelihood values, and proceed to the next site. In many cases, moving to the next site will also involve a change in the tree topology, hence we redistribute the compressed likelihoods accordingly using logic common to other tree sequence algorithms[28,29]. For simplicity, the current implementation only allows for exact haplotype matching. Under this assumption, we need only five discrete values to encode the node likelihoods in the LS Viterbi algorithm, simplifying the logic considerably. Methods to incorporate mismatch and integration with tskit are currently underway.

To validate the correctness of our implementation of the copying process, we devised a strong test, referred to as perfect inference, under which the correct tree sequence should be inferred. We begin with a simulated tree sequence with no mutations and derive the true ancestral segments from it. We then add a specific pattern of mutations that are designed to precisely identify the end points of each ancestor and use the resulting ancestral haplotypes as input to tsinfer. We then find copying paths for these ancestors and samples in the usual way. Using this method, we are able to reproduce the input tree sequence topology perfectly, recovering every marginal tree and recombination breakpoint exactly for arbitrarily large inputs. Indeed, the numerical tables[29] representing the input and output tree sequences are byte-for-byte identical. Although not a formal proof, this identity holds for all tested inputs. It also strongly suggests that the key areas for further research are better ways to infer ancestral haplotypes and demarcate their end points.

Path compression. The algorithm for inferring ancestors discussed above is primarily based on the signal that arises from shared mutation events, and is only weakly informed by recombination. However, we can also derive information about ancestors from shared recombination events. If we assume that each recombination event is unique, that is, that all samples that inherit the local haplotype resulting

from a breakpoint did so from a single ancestor, we can then estimate the state of this ancestor. Note that this is equivalent to assuming an infinite-sites-like model for recombination events, an idea with a long history[51]. We use this signal of shared recombination breakpoints in a specific way, which we refer to as path compression.

When generating copying paths for successive ancestors, we often find that subsets of two or more paths are identical. Such identical path subsets are evidence for the existence of a single ancestor that consisted of the concatenation of the corresponding haplotype segments. We therefore add this synthetic ancestor, and adjust the original identical path subsets to copy from the newly inserted ancestor. Ancestors corresponding to a given allele age are inserted at the same time, and path compression is run at the end of each of these time slices. Supplementary Figure 17 shows an illustrative example of this process.

Inference accuracy. To compare the accuracy of tsinfer to other inference methods, we used simulations to generate known topologies. We assessed the effect of genotyping errors on inference accuracy by simulating errors on the haplotypes using an empirically determined genotyping error profile[48]. We then provided the corresponding haplotypes (with and without simulated genotyping errors) to the various tools, and measured the difference between the estimated and true tree topologies using tree distance metrics. We considered four tools: tsinfer, ARGweaver, Rent+ and fastARG. ARGweaver requires several parameters to be specified: in all cases we used the known simulation values for mutation rate, recombination rate and effective population size parameters, and used the default number of time steps for time discretization (20), sampling 10 ARGs for each simulation (one every 20 Markov chain Monte Carlo cycles, after a burn-in period of 1,000 cycles).

Although the succinct tree sequence data structure can fully represent node timing (and hence branch length) information, tsinfer does not currently attempt to infer the precise times of ancestors. Therefore, we limited our investigation of the accuracy of inference to assessing the quality of the inferred topologies using tree distance metrics. For each replicate simulation, we computed the average distance between pairs of true and inferred trees along the sequence, weighted by the distance along the sequence that these trees persist. We report the average distance over replicate simulations. Metrics were calculated using the R packages treespace[52] and phangorn[53]. Some metrics (such as Robinson–Foulds) are undefined for trees that contain nonbinary nodes (that is, polytomies), which indicate uncertainty in tsinfer and therefore occur frequently. We therefore also show results for which the tsinfer trees have been randomly resolved into fully bifurcating trees (averaged over 10 replicates). The Kendall–Colijn metric[40] provides the greatest discrimination (Supplementary Fig. 4) and is well-defined for all tree topologies, and was therefore used exclusively in subsequent analyses. At low mutation rates, the Kendall–Colijn metric shows a notable difference between the accuracy of the trees inferred by tsinfer before versus after random resolution of polytomies. This is because there is little information available to resolve the nodes, and generating a random binary subtree on average results in something further from the truth than the original polytomy. Thus, the innate strategy of tsinfer of using polytomies to indicate uncertainty in a principled and systematic way has a considerable advantage over methods that always fully resolve trees.

To evaluate the sensitivity of tsinfer to changes in the underlying simulation model, we also tested accuracy on more complex simulations. In Supplementary Fig. 6, we show results of simulations of a three-population out-of-Africa model of human demography[54]. In this case, tsinfer does not seem to be affected by the underlying population structure and is a little more accurate than ARGweaver (although ARGweaver is less affected by error). In Supplementary Fig. 7, we show inference accuracy on a simulated selective sweep, for which we performed forward time simulations using SLiM[55,56]. In this case, once the advantageous mutation has swept to a reasonable frequency, tsinfer becomes substantially more accurate than the other tools and continues to be so for many generations after fixation. In Supplementary Fig. 18, we show the effect of running inference on a subset of the available haplotypes on the accuracy of tsinfer. We find that, in the absence of error, having extra samples has little effect on the accuracy of inference, but that larger samples can potentially help to correct for the presence of genotyping errors.

To evaluate the computational performance of the different inference methods, we measured the total user time and maximum memory usage (taking the mean over replicates). All experiments were run on a server with two Xeon E5-2680 CPUs and 256 GB of RAM. Supplementary Figure 8 shows the CPU time required for all four tools for varying sample sizes. The disparity in the running times is too large to show on a single scale, and tsinfer and fastARG are many times faster than ARGweaver and Rent+. Supplementary Figure 9 compares tsinfer and fastARG at a much larger scale, for which tsinfer shows far better scaling in terms of CPU time and memory when increasing both sequence length and sample size. Empirically, the running time of tsinfer grows approximately linearly with sample size and super-linearly with sequence length on simulated data (Supplementary Fig. 9).

All code for running the evaluations, including the precise version of each tool used, is included in the accompanying GitHub repository (https://github.com/mcveanlab/treeseq-inference/).

Genealogical nearest neighbors. We use GNN, a statistic based on the topological properties of trees and defined with respect to a collection of reference sets, to summarize the identity of nearest neighbors (Supplementary Fig. 19). For a given tree and focal node u, GNN values are computed by traversing upward from u until we find a target node v that has one or more descendants (not including u) present in any of the reference sets. The GNNs are then the proportions of each reference set among the descendants of v, not including u.

More formally, let R be a list of K sets of reference nodes and let $C^t_{v,k}$ be the number of nodes descending from (and including) v in tree t from the set R_k, with $C^t_v = \sum_{k=1}^{K} C^t_{v,k}$. For a given focal node u and tree t, the GNN statistic is then defined as

$$G^t_{u,k} = \frac{C^t_{v,k} - [u \in R_k]}{C^t_v - \delta(u)}$$

where $[\mathbf{x}]$ is an Iversonian condition such that $[\mathbf{x}] = 0$ if $\mathbf{x}$ is false and $[\mathbf{x}] = 1$ otherwise; $\delta(u) = [u \in \bigcup_{j=1}^{K} R_j]$; and v is the first node on the path from u to root in t such that $C^t_v > \delta(u)$. The average GNN along a tree sequence $\mathbb{T}$ is

$$G_{u,k} = \frac{1}{L} \sum_{t \in \mathbb{T}} L^t G^t_{u,k}$$

where each tree $t \in \mathbb{T}$ covers a span of L^t units of genetic sequence and $L = \sum_{t \in \mathbb{T}} L^t$. Thus, the average GNNs are equal to the treewise GNN values weighted by the genomic span of each tree.

Note that if the reference sets do not include all leaf nodes in a tree, the sister clade to a leaf u may not contain any individuals in a reference set. In this case we will ascend to an older target node v, higher in the tree, and the GNN statistic will represent a more distant relationship.

Data visualization. Data processing was performed using the Python data science stack including numpy[57], pandas[58], matplotlib[59] and seaborn (https://doi.org/10.5281/zenodo.1313201).

Figure 5 shows patterns of genetic relatedness in UKB on a map of Britain and Ireland. We grouped birth locations for individuals according to the NUTS 2018[60] classification. Reverse geocoding of birth locations was performed for all 444,848 UKB participants with recorded birth coordinates using bng_latlon (https://pypi.org/project/bng-latlon/) and Shapely (https://pypi.org/project/Shapely/). In total, 8,315 samples, for which NUTS-2 birth locations were not found or did not tally with their reported country of birth, were removed. A different GNN matrix was computed for the NUTS-2 (Fig. 5a,b) and NUTS-3 (Fig. 5c–e) mappings. Maps were drawn with cartopy (http://scitools.org.uk/cartopy) using publicly available vector shape data. Shape data for NUTS areas was provided by the Office for National Statistics (https://data.gov.uk/) under the Open Government License. Shape data for the coastal outline of Ireland were downloaded from the Database of Global Administrative Areas, which are free to use for academic publishing (https://gadm.org/license.html).

Reporting Summary. Further information on research design is available in the Nature Research Reporting Summary linked to this article.

Data availability

The TGP[30], SGDP[31] and UKB[32] datasets used here are detailed in the relevant publications. Tree sequences inferred for all TGP (https://doi.org/10.5281/zenodo.3052359) and SGDP (https://doi.org/10.5281/zenodo.3052359) autosomes have been deposited on Zenodo. Tree sequences were compressed using the tszip utility; see the documentation at https://tszip.readthedocs.io/ for further details.

Code availability

tsinfer is freely available under the terms of the GNU GPL; see the documentation at https://tsinfer.readthedocs.io/ for further details. All code used to process data and run evaluations is available at https://github.com/mcveanlab/treeseq-inference.

References

43. Kimura, M. & Ota, T. The age of a neutral mutant persisting in a finite population. *Genetics* **75**, 199–212 (1973).
44. Griffiths, R. C. & Tavaré, S. The age of a mutation in a general coalescent tree. *Stoch. Models* **14**, 273–295 (1998).
45. Ormond, L., Foll, M., Ewing, G. B., Pfeifer, S. P. & Jensen, J. D. Inferring the age of a fixed beneficial allele. *Mol. Ecol.* **25**, 157–169 (2016).
46. Nakagome, S. et al. Estimating the ages of selection signals from different epochs in human history. *Mol. Biol. Evol.* **33**, 657–669 (2016).
47. Smith, J., Coop, G., Stephens, M. & Novembre, J. Estimating time to the common ancestor for a beneficial allele. *Mol. Biol. Evol.* **35**, 1003–1017 (2018).
48. Albers, P. K. & McVean, G. Dating genomic variants and shared ancestry in population-scale sequencing data. Preprint at *bioRxiv* https://doi.org/10.1101/416610 (2018).
49. Keightley, P. D. & Jackson, B. C. Inferring the probability of the derived vs. the ancestral allelic state at a polymorphic site. *Genetics* **209**, 897–906 (2018).

50. Lunter, G. Haplotype matching in large cohorts using the Li and Stephens model. *Bioinformatics* **35**, 798–806 (2019).
51. Fisher, R. A. A fuller theory of 'junctions' in inbreeding. *Heredity* **8**, 187–197 (1954).
52. Jombart, T., Kendall, M., Almagro-Garcia, J. & Colijn, C. treespace: statistical exploration of landscapes of phylogenetic trees. *Mol. Ecol. Resour.* **17**, 1385–1392 (2017).
53. Schliep, K. P. phangorn: phylogenetic analysis in R. *Bioinformatics* **27**, 592–593 (2011).
54. Gutenkunst, R. N., Hernandez, R. D., Williamson, S. H. & Bustamante, C. D. Inferring the joint demographic history of multiple populations from multidimensional SNP frequency data. *PLoS Genet.* **5**, e1000695 (2009).
55. Haller, B. C. & Messer, P. W. SLiM 3: forward genetic simulations beyond the Wright–Fisher model. *Mol. Biol. Evol.* **36**, 632–637 (2019).
56. Haller, B. C., Galloway, J., Kelleher, J., Messer, P. W. & Ralph, P. L. Tree-sequence recording in SLiM opens new horizons for forward-time simulation of whole genomes. *Mol. Ecol. Resour.* **19**, 552–566 (2019).
57. Oliphant, T. E. *A guide to NumPy* (Trelgol Publishing, 2006).
58. McKinney, W. et al. Data structures for statistical computing in Python. *Proc. 9th Python in Science Conference* 51–56 (2010).
59. Hunter, J. D. Matplotlib: a 2D graphics environment. *Comput. Sci. Eng.* **9**, 90 (2007).
60. *Regions in the European Union–Nomenclature of Territorial Units for Statistics–NUTS 2013/EU-28* (Eurostat, 2011).

nature research

Corresponding author(s): Jerome Kelleher

Last updated by author(s): Jul 9, 2019

Reporting Summary

Nature Research wishes to improve the reproducibility of the work that we publish. This form provides structure for consistency and transparency in reporting. For further information on Nature Research policies, see Authors & Referees and the Editorial Policy Checklist.

Statistics

For all statistical analyses, confirm that the following items are present in the figure legend, table legend, main text, or Methods section.

n/a	Confirmed	
☐	☒	The exact sample size (*n*) for each experimental group/condition, given as a discrete number and unit of measurement
☐	☒	A statement on whether measurements were taken from distinct samples or whether the same sample was measured repeatedly
☒	☐	The statistical test(s) used AND whether they are one- or two-sided *Only common tests should be described solely by name; describe more complex techniques in the Methods section.*
☒	☐	A description of all covariates tested
☐	☒	A description of any assumptions or corrections, such as tests of normality and adjustment for multiple comparisons
☒	☐	A full description of the statistical parameters including central tendency (e.g. means) or other basic estimates (e.g. regression coefficient) AND variation (e.g. standard deviation) or associated estimates of uncertainty (e.g. confidence intervals)
☒	☐	For null hypothesis testing, the test statistic (e.g. *F*, *t*, *r*) with confidence intervals, effect sizes, degrees of freedom and *P* value noted *Give P values as exact values whenever suitable.*
☒	☐	For Bayesian analysis, information on the choice of priors and Markov chain Monte Carlo settings
☒	☐	For hierarchical and complex designs, identification of the appropriate level for tests and full reporting of outcomes
☒	☐	Estimates of effect sizes (e.g. Cohen's *d*, Pearson's *r*), indicating how they were calculated

Our web collection on statistics for biologists contains articles on many of the points above.

Software and code

Policy information about availability of computer code

Data collection	All code used to collect simulated data is available at https://github.com/mcveanlab/treeseq-inference
Data analysis	All code used to analyse simulated and human data is available at https://github.com/mcveanlab/treeseq-inference. Tsinfer is licensed under the GNU GPL and available at https://pypi.org/project/tsinfer/

For manuscripts utilizing custom algorithms or software that are central to the research but not yet described in published literature, software must be made available to editors/reviewers. We strongly encourage code deposition in a community repository (e.g. GitHub). See the Nature Research guidelines for submitting code & software for further information.

Data

Policy information about availability of data

All manuscripts must include a data availability statement. This statement should provide the following information, where applicable:

- Accession codes, unique identifiers, or web links for publicly available datasets
- A list of figures that have associated raw data
- A description of any restrictions on data availability

This work uses data from the UK Biobank, 1000 Genomes Project and Simons Genome Diversity Project, all of which are cited in the text. All details of how these are used and processed are described at https://github.com/mcveanlab/treeseq-inference.

Field-specific reporting

Please select the one below that is the best fit for your research. If you are not sure, read the appropriate sections before making your selection.

☒ Life sciences ☐ Behavioural & social sciences ☐ Ecological, evolutionary & environmental sciences

For a reference copy of the document with all sections, see nature.com/documents/nr-reporting-summary-flat.pdf

Life sciences study design

All studies must disclose on these points even when the disclosure is negative.

Sample size	Sample sizes were determined by the available data in UKB, 1000G and SGDP datasets.
Data exclusions	In the SGDP dataset, we removed one individual due to a lack of metadata. We considered only simple, biallelic SNPs across all three datasets.
Replication	Our findings illustrate the utility of the tsinfer method, and are reproduced by applying the method to three, very different, human datasets.
Randomization	Randomization is not relevant to this study because we are investigating the utility of the tsinfer method.
Blinding	Blinding is not relevant to this study because we are investigating the utility of the tsinfer method.

Reporting for specific materials, systems and methods

We require information from authors about some types of materials, experimental systems and methods used in many studies. Here, indicate whether each material, system or method listed is relevant to your study. If you are not sure if a list item applies to your research, read the appropriate section before selecting a response.

Materials & experimental systems

n/a	Involved in the study
☒	☐ Antibodies
☒	☐ Eukaryotic cell lines
☒	☐ Palaeontology
☒	☐ Animals and other organisms
☐	☒ Human research participants
☒	☐ Clinical data

Methods

n/a	Involved in the study
☒	☐ ChIP-seq
☒	☐ Flow cytometry
☒	☐ MRI-based neuroimaging

Human research participants

Policy information about studies involving human research participants

Population characteristics	Data are from the UKB, 1000G and SGDP datasets, which are fully characterized in the cited publications.
Recruitment	Data are from the UKB, 1000G and SGDP datasets, which are fully characterized in the cited publications.
Ethics oversight	Data are from the UKB, 1000G and SGDP datasets, which are fully characterized in the cited publications.

Note that full information on the approval of the study protocol must also be provided in the manuscript.